Environmental correlates of Arctic ice-edge noise

Nicholas C. Makris[a] and Ira Dyer
Department of Ocean Engineering, Massachusetts Institute of Technology, Cambridge, Massachusetts 02139

(Received 5 February 1991; accepted for publication 8 July 1991)

Temporal variations of low-frequency, broadband ambient noise measured in early summer under drifting ice floes of the marginal ice zone (MIZ) are cross correlated with local environmental forces and ice field descriptors. Surface gravity wave forcing is the primary correlate of the noise; its interaction with ice floes generates sound, most likely via flexural floe failure, and unloading motion, within a few kilometers of the ice edge. Ice concentration is also well correlated with the noise, most likely parametrically. That is, as ice concentration increases, so does the density of potential sound sources in the ice field. Ice stress, ice moment, and wind stress magnitude, while highly correlated with low-frequency noise in the fully ice-covered Arctic, are poor correlates in the MIZ. Lateral melt rate, as a surrogate for thermally induced ice stress, is also poorly correlated with low-frequency MIZ noise. When surface wave forcing is weak, about 1/2 the time in this experiment, episodes of high noise are sometimes observed. These episodes are roughly 3–6 h in duration and 12 h in periodicity. Evidence suggests that they are related to the formation and advection of bands of highly concentrated ice by internal waves during off-ice winds.

PACS numbers: 43.30.Ma, 43.30.Nb

SYMBOLS FOUND IN TABLES

Symbols used specifically in the tables are defined here. Subscripts x,y denote east and north components respectively.

$\|P\|$	ambient noise rms pressure in the 25- to 50-Hz band
τ_a	wind stress vector
τ_w	current stress vector
V_i	ice drift velocity vector
V_g	absolute current velocity vector at 50-m depth
σ_p	pressure gradient shear stress vector
M_r	lateral melt rate
SW	surface gravity wave amplitude
$\dot{\epsilon}_{\text{div}}$	ice field divergence rate
$\dot{\epsilon}_{12}$	ice field shear strain rate
$\dot{\epsilon}_{xx} - \dot{\epsilon}_{yy}$	ice field east–west expansion rate
C	ice field concentration
$\epsilon_{xx} - \epsilon_{yy}$	ice field east–west expansion
ω_{abs}	ice field rotation rate
$(\dot{\epsilon}_{\text{div}})^2 + (\dot{\epsilon}_{12})^2$	ice field deformation energy

INTRODUCTION

As part of the marginal ice zone experiment of 1984 (MIZEX 84), MIT measured ambient noise beneath freely drifting ice floes. These measurements were made in the Fram Strait near 80.5° N and 8° E, during the month of June. Our purpose in acquiring the data is to gain an understanding of the physical mechanisms responsible for marginal ice zone (MIZ) underwater noise.

In this paper, we compare temporal variations of low-frequency ambient noise with environmental forces applied to the ice, including those due to wind, current, drift, surface gravity wave amplitude and heat flux. We find that over long periods, about 3 h or more (autocorrelation e-folding time), low-frequency MIZ noise cross correlates best with surface gravity wave amplitude. Surface gravity waves penetrate into the MIZ from the open waters of the East Greenland Sea, and are primarily responsible for the break-up of ice floes.

We also compare temporal variations of the noise with certain ice descriptors. These include ice concentration, deformation, and deformation rate. We find that, over long periods, the noise is well correlated with ice concentration. For the shorter periods, and when surface wave forcing is weak, episodes of high noise are sometimes observed. These episodes are of 1- to 2-h autocorrelation time (3- to 6-h duration) and 12-h periodicity. Qualitative evidence suggests that they are related to the formation and advection of bands of highly concentrated ice by internal waves. Together, these findings suggest that low-frequency ambient noise is parametrically dependent upon ice concentration in the MIZ, over both short and long periods. In particular, we suggest that as ice concentration increases, so does the density of potential surface sound sources.

Over long periods internal ice stress, applied moment, and the individual stresses resulting from wind, current, and

[a] Presently at Naval Research Laboratory, Washington, DC 20375.

 0001-4966/91/123288-11$00.80

drift are generally poor correlates of noise in the MIZ. This is in contrast to the results of Makris and Dyer[1] for pack-ice-covered waters of the central Arctic. We interpret this difference to be a direct consequence of the reduced fetch available for normal horizontal stress and moment accumulation in the MIZ. That is, decreased ice floe size and less than continuous ice cover, as well as the proximity of the ice edge, where normal horizontal stresses may be relieved, are primarily responsible for the reduction of ice stress in the MIZ with respect to the central Arctic.

Diachok and Winokur[2] first showed that ambient noise of the MIZ could vary from that of the adjacent open ocean and pack-ice-covered seas. Via a series of across ice-edge synoptic (2 h) sonobuoy measurements, they observed increased noise levels at or near the ice edge, which they attributed to surface gravity wave interaction with ice floes. From measurements made via a towed array, within a 1-day period, Yang *et al.*[3] more recently found the along ice-edge distribution of noise to be localized at "hotspots" of less than 5-km length and about 50-km spacing. They speculated that ice-edge eddies may have been responsible for the hotspots, although they lacked environmental data to support this. Subsequently, Johannessen *et al.*[4] synoptically measured ambient noise levels with sonobuoys, within a 6-h period, in a region containing two mesoscale eddies, and found indications of hotspots, although their spatial sampling interval was at roughly five times the reported hotspot size. In contrast, the present study has longer noise records, finer spatial sampling of the noise field and a wider range of environmental data, but it was carried out in a region with no apparent eddy motion, and did not include observations either in the adjacent open water or fully covered central Arctic ice field.

Lewis and Denner[5] have studied the relationship between noise and heat flux. They have found that episodes of high noise in the frequency range up to several kHz correlate well with heat flux. This mechanism is thought to be important when thermal changes are large, as is the case in the Arctic for most of the year, but typically not in the summer. Because of the summer season, and the lower frequency range considered, the MIZEX 84 noise data we have studied are unlikely to relate to heat flux. But it is, nonetheless, included here as a possible environmental correlate.

Acoustic measurements were made using hydrophones suspended at 60 m below freely drifting ice floes. While up to 24 such hydrophones were deployed, roughly half this number were within our operational rf telemetry range at a given time. The operational phones formed a typically 5-km scale random array. In response to a wide range of wind and current magnitudes and directions, this array drifted within 5–20 km of relatively open water. Via an integral sensor tracking system (STS),[6,7] floes equipped with acoustic sensors and current meters could be located. These locations were also used to calculate ice field descriptors such as concentration and strain. Wind and drift measurements were made from the experiment base ship Kvitbjorn (Kv), which was part of the STS. While the ice-edge position, roughly normal to the concentration gradient, varied by tens of kilometers over the course of the roughly 2 week acoustic experiment, it maintained an east–west orientation within 20 km of the Kv. Charts of geostrophic current and microwave imagery show that there were no prominent mesoscale eddies in this vicinity at any time during the experiment.[8–10] This was confirmed via ice kinematic data.[11]

Noise in a 25- to 50-Hz band is used as a surrogate for the broad distribution of low-frequency ambient noise, as may be justified by inspection of Fig. 1, which indicates that this band is at or near the peak of the noise spectrum. Spectra from about 5 to 300 Hz at other times increased or decreased nearly uniformly, so that the octave containing the peak closely mimics temporal variations of the low-frequency spectrum.

Records of rms noise in the 25- to 50-Hz band were constructed from the analog and digital recordings of each available drifting sensor. The noise records of two of the most consistently operational sensors appear in Fig. 2, and were obtained by integrating and then square rooting the pressure spectral density over the 25- to 50-Hz band. The averaging period for each sample varied from 1 to 5 min. The sampling interval of these long-term noise records was no greater than 1/2 h, and sometimes finer. Gaps in the ambient noise records were caused by contamination from interfering acoustic experiments, and intermissions in recording, the statistics of which appear in Table I. Due to a long, roughly 3-day intermission in recording, the noise records occurring before and after this intermission have been analyzed separately. They are respectively referred to as the first and second drift phases.

By comparing the noise records of the two sensors

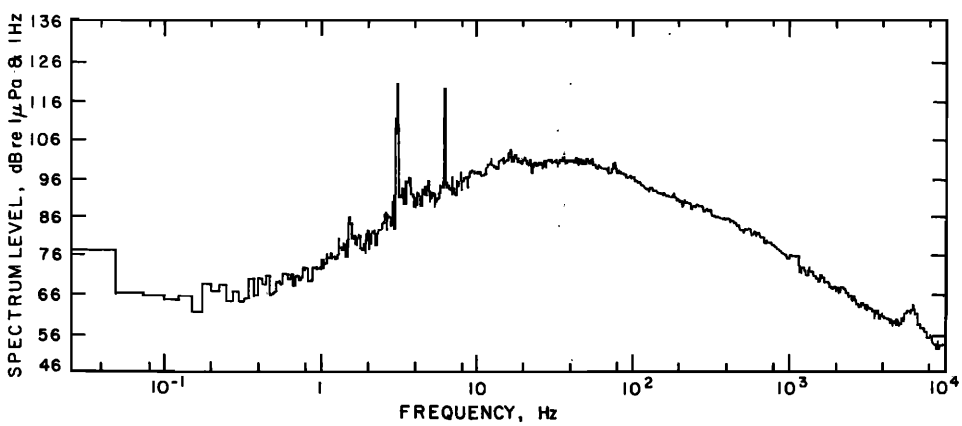

FIG. 1. Composite of ambient noise observed on Julian Day 177.4 with sensor D2. Data were taken sequentially over several decades in frequency, and then repeated to cover adjacent decadal ranges. All data were acquired within 1/2 h. Peaks at about 3 and 6 Hz are caused by hydrophone cable strum. The broad peak from about 5 to 7 kHz is an artifact associated with the cable/preamplifier electronics, and should be ignored. A 40-dB/decade high-pass filter with corner frequency at $f = 1$ Hz has whitened the noise for $f < 1$ Hz, and should be corrected for upon use of this graph in this frequency range.

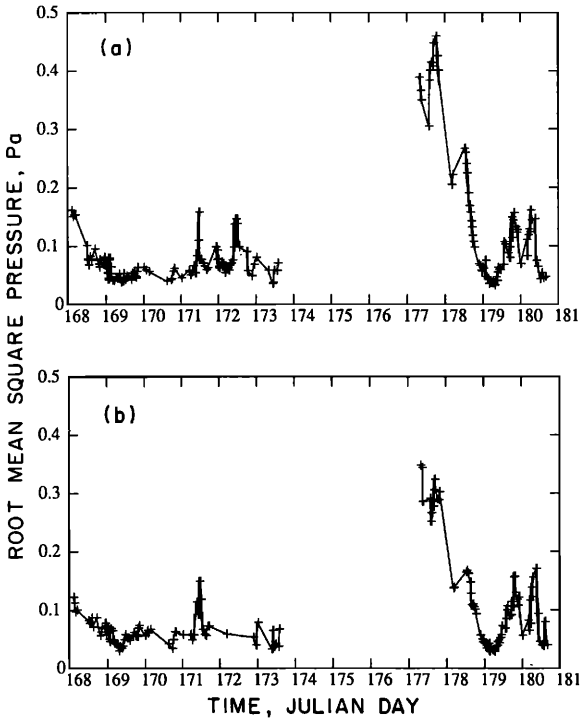

FIG. 2. Root-mean-square noise in the 25- to 50-Hz band for sensors (a) D6 and (b) D24. These sensors were separated by between 1.5 to 5.0 km throughout the time period shown. Pluses indicate data points within each of two separate drift phases. The first drift phase, from J168 to J174 has a mean of 0.07 and 0.06 Pa and a standard deviation of 0.03 and 0.02 Pa for (a) and (b), respectively. The second drift phase, from J177 to J181, has a mean of 0.15 and 0.12 Pa and a standard deviation of 0.12 and 0.09 Pa for (a) and (b), respectively.

shown in Fig. 2, it is evident that long-term temporal variations of the noise are nearly uniform over the roughly 5-km region occupied by the acoustic array. This observation is quantitatively confirmed via cross correlation of the respective noise records. A peak correlation coefficient of 0.79 was obtained during the first drift phase and 0.97 during the second, each at zero time lag. The cross-correlation algorithm that we used required no interpolation of data gaps and so introduced no hypothetical information. This algorithm, described in the Appendix, was used for all auto and cross

TABLE I. Gap statistics for long-term noise records.

Record sensor	drift phase	Mean gap (h)	Longest gap (h)	% gap
D6	1st	2.3	10.4	41
D24	1st	3.3	14.4	53
D6	2nd	2.3	7.0	34
D24	2nd	2.3	7.0	34

correlations in this paper. Because the noise record for sensor D6 was better sampled during the first drift phase, it is used exclusively in this paper for correlations with environmental records.

More densely sampled acoustic data measured during a particular high noise episode, from an array consisting of several hydrophones, are analyzed in Sec. III.

I. NOISE AUTOCORRELATION TIME IS SHORTER IN THE MIZ

Time series of the rms noise, as shown in Fig. 2(a) have been autocorrelated for each of the drift phases, and are shown in Fig. 3. Spectra are also given. The e-folding time (the time at which the normalized autocorrelation falls to e^{-1}) for the two are listed in Table II, at 3 and 13 h, respectively. These are considerably shorter than observed for the central Arctic, about 29 h.[1] Therefore, the available data indicate that the MIZ is an acoustically more dynamic region which, of course, is a consequence of the greater dynamism of the MIZ environment.

Spectral slopes shown in Fig. 3 for large values of ν are about ν^{-2}, and compare with $\nu^{-3/2}$ for the central Arctic.[1] No strong semidiurnal or diurnal components are observed in either, although an argument can be made for a weak semidiurnal component during the first drift phase. The faster evolution of the first drift phase, compared to the second, shows in its spectrum as well as in its autocorrelation time.

While the spectra have no strong semidiurnal components, we will show in Sec. III that such components can sometimes be observed. What is required is the absence of

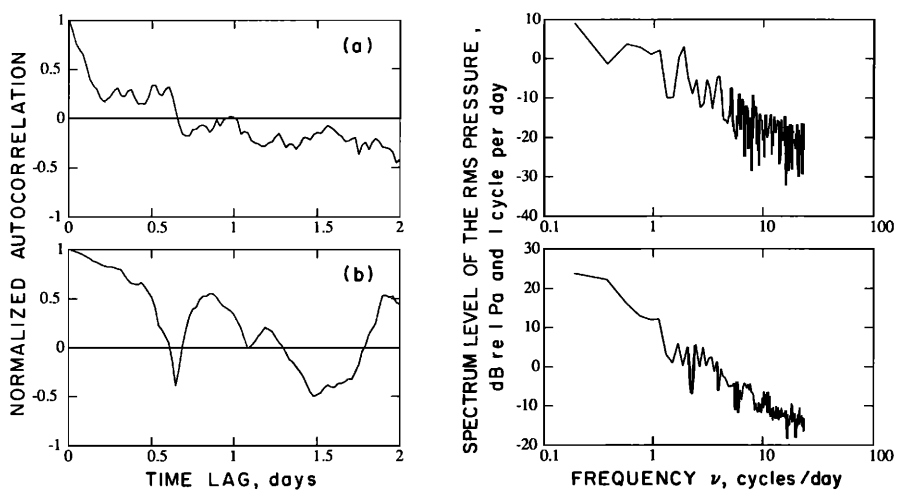

FIG. 3. The time lagged normalized autocorrelation and spectral level of the 25- to 50-Hz rms noise as measured by sensor D6 for (a) the first drift phase, (b) the second drift phase. For the first drift phase, a 3-h e-folding time is measured and a spectral peak at $\nu = 2$ cycle/day can be argued for in the spectrum, corresponding to the oceanographically important period of inertial oscillations. For the second drift phase a 13-h e-folding time is measured and there is no evidence of a spectral peak at 2 cycle/day.

surface wave forcing, the major factor in noise generation (Sec. II), and other environmental effects that concentrate the ice (Sec. III).

II. SURFACE GRAVITY WAVES CORRELATE BEST WITH THE NOISE

A. Environmental forcing functions

A variety of dynamical forcing functions were cross correlated with the noise. These include horizontal wind shear stress which acts on the upper surface of the ice, current shear stress which acts on the lower surface, normal stress applied by the Coriolis, and lineal acceleration forces which act uniformly on an ice floe's submerged section, lateral melt rate as a surrogate for heat flux, and surface gravity wave amplitude. Each of these, individually or in combination, can cause ice fracture and, hence, noise.

The following expressions describe the horizontal stresses acting upon a drifting ice floe, as induced by wind, current, and drift. These are similar to those found in Makris and Dyer.[1] In particular, wind speed $|\mathbf{V}_a|$ measured on board the Kv 10 m above the ice was averaged over and sampled at 10-min intervals, and converted to wind shear stress via

$$\boldsymbol{\tau}_a = c_{10}\rho_a|\mathbf{V}_a|\mathbf{V}_a,$$

where ρ_a is air density and $c_{10} = 0.0023$ is the air–ice drag coefficient corresponding to neutrally stable conditions encountered during MIZEX 84.[12] Current velocity relative to the drifting ice $\mathbf{V}_w$ measured at 10-m depth and averaged over and sampled at 10-min intervals, were converted to current stress magnitude via

$$|\boldsymbol{\tau}_w| = c_w\rho_w|\mathbf{V}_w|^2,$$

where $c_w = 0.0046$ is the ice-ocean drag coefficient based upon measurements at 10-m depth, and ρ_w is the density of sea water. The ice-ocean shear stress is rotated clockwise downward through the oceanic boundary layer with inflow angle

$$\cos\alpha = \boldsymbol{\tau}_w\cdot\mathbf{V}_w/|\boldsymbol{\tau}_w||\mathbf{V}_w|, \quad \alpha = -28°,$$

where the numerical value has been determined by Makris.[11]

Coriolis normal stress is derived from

$$\boldsymbol{\sigma}_c = -2\rho_i h\Omega(\sin\phi)(\mathbf{i}\times\mathbf{V}_i),$$

where $\mathbf{V}_i$ is the ice drift velocity, ρ_i is the ice density, h is the ice sheet thickness, taken to be 1.5 m, ϕ is the latitude, Ω is the Earth's angular speed, and $\mathbf{i}$ is a unit vector in the vertical. Ice drift velocity was obtained by Kalman filtering satellite navigation data for the Kv with a 6-h low-pass filter to hourly values[13] which were later interpolated to half hourly values by us. The normal stress associated with lineal acceleration, $\rho_i h(d\mathbf{V}_i/dt)$, was determined by differentiating the low-pass drift velocity. The normal stress applied by the pressure gradient force is

$$\boldsymbol{\sigma}_p = 2\rho_w h_s\Omega(\sin\phi)(\mathbf{i}\times\mathbf{V}_g) + \rho_w h_s\frac{d\mathbf{V}_g}{dt},$$

where h_s is the submerged thickness of the ice sheet and $\mathbf{V}_g$ is the absolute current velocity. It is measured at 50-m depth where momentum transfer from the Ekman layer is assumed to be negligible. The lineal acceleration term is of the same order as the geostrophic term due to rapidly varying currents in the MIZ.

The internal ice stress acting normal to the ice sheet's vertical section is approximated as[1]

$$\mathbf{S} = (\boldsymbol{\tau}_a + \boldsymbol{\tau}_w)(L_s/h)$$

where the combined contributions of Coriolis, pressure gradient, and lineal acceleration normal horizontal stresses are negligible for our experiment. The stress moment acting about the ice sheet's central horizontal plane is approximated as[1]

$$\mathbf{M} = \mathbf{i}\times(\boldsymbol{\tau}_a + \boldsymbol{\tau}_w)(L_m/2).$$

Lengths parallel to $\mathbf{S}$ and normal to $\mathbf{M}$ are L_s and L_m, respectively, through which horizontal load and bending moment may be accumulated. We estimate L_s to be less than or equal to a few floe lengths or no more than about 500 m, and L_m to be less than or equal to a typical floe length or no more than about 100 m.

Lateral melt rate, M_r, is assumed to be roughly proportional to $\Delta T_w^{1.36}$,[14] where $\Delta T_w = T_w - T_f$ is the elevation of sea temperature above freezing at $T_f = -1.98$ °C. Sea temperature T_w was measured at 5 m below sea level, and averaged and sampled at 10-min intervals.[13] For our experiment, M_r is a surrogate for heat flux.

We computed the surface gravity wave field in the East Greenland Sea adjacent to the ice edge from contemporary meteorological charts via the Pierson *et al.* spectral method.[15] This proved to be quite simple since only on-ice winds have sufficient fetches to generate potentially important surface wave amplitudes at the ice edge. Surface wave amplitudes within the MIZ, at the acoustic array, were determined for wave periods in excess of 8 s from empirically and theoretically derived attenuation coefficients,[16] and estimates of the array's distance from the ice edge. Waves in this period regime are subsequently referred to as swell, at least because wind stress in the ice field no longer drives the gravity waves. We did not consider waves with periods shorter than 8 s because investigations of flexural floe failure by Goodman *et al.*;[17] and high-frequency floe collisions ($\approx$1 Hz) in the MIZ by Martin and Becker[18] indicate that surface waves in the swell regime (periods $\geqslant$8 s) are primarily responsible. In addition, earlier work by Diachok indicates the higher the wave period, the more intense the low-frequency noise.[19]

The e-folding autocorrelation times of the ice-forcing functions are summarized in Table II. During the first drift phase, the roughly 3-h time scale of the noise was most similar to time scales of stresses derived from ice drift and current. Of these, only drift speed (Fig. 4) and current stress (not shown) display evidence of semidiurnal peaks in their spectra, as does the noise, the latter only weakly. During the second drift phase, the e-folding time of the noise increased by nearly a factor of 4. It is much shorter than the e-folding time calculated for surface waves, but longer than that measured for wind stress magnitude.

Results of cross correlation between dynamical forcing

TABLE II. Autocorrelation e-folding times for noise and environmental forcing functions, in hours. (Data sampled at 1/2-h intervals.) Incomplete environmental data in the second drift phase account for the lack of some entries.

	1st drift	2nd drift
$\|P\|$	3	13
$\|\tau_a\|$	8	6
$\|\tau_w\|$	2	
$\|\tau_a + \tau_w\|$	5	
$\|\tau_a - \tau_w\|$	4	
$\|\mathbf{V}_i\|$	4	4
$\|d\mathbf{V}_i/dt\|$	3	3
$\|\sigma_p\|$	3	
M_r	19	
SW	23	48

TABLE III. Cross correlations between ambient noise (rms pressure) in the 25- to 50-Hz band and environmental forcing functions. Environmental time series are held fixed. (Data sampled at 1/2-h intervals.) [Peak correlation coefficient, time lag (h).]

	1st drift $\|P\|$	2nd drift $\|P\|$
$\|\tau_a\|$	0.15, −1.5	0.56, 0
$\|\tau_w\|$	0.35, −0.5	
$\|\tau_a + \tau_w\|$	0.25, −1.0	
$\|\tau_a - \tau_w\|$	0.23, −0.5	
$\|\mathbf{V}_i\|$	0.13, 1.0	−0.27, 2.6
$\|d\mathbf{V}_i/dt\|$	−0.06, 2.0	
$\|\sigma_p\|$	0.23, −2.5	
M_r	0.26, 3.0	
SW	0.60, 0	0.93, 0

functions and noise are summarized in Table III. During both drift phases, surface gravity wave amplitude is by far the best correlate of the noise, supporting this as a general result. The lower correlation found during the first drift phase is primarily due to episodes of high noise which occur during weak surface wave activity. Evidently, these noise episodes are not caused by surface waves. They will be discussed in Sec. III.

Figures 4 and 5, for the first and second drift phases respectively, show time series for measured noise and calculated surface wave amplitude. Visual comparison of the two supports the cross-correlation results of Table III, from which we have concluded that surface wave correlation is the best. Another environmental force that has scored well in Table III (wind stress) is also shown, as is ice concentration (to be discussed subsequently). Arguments in favor of these clearly can be made, and we will do so for ice concentration, but wind stress is a far less consistent correlate, and does come out second best to surface waves.

The primary cause for the break-up of ice floes in the MIZ is surface-wave-induced flexural failure, as may be surmised from the work of Goodman *et al.*[17] Their results are the basis for Fig. 6, which gives the surface wave amplitude required for flexural failure. Comparing Figs. 4 and 5 with Fig. 6, we observe that surface gravity wave amplitudes were sufficient to cause flexural floe failure within several kilometers of the ice edge during at least some periods of high noise within each drift phase. Low-frequency sound then could have been radiated into the water via the fracture itself and from unloading motion of ice floes once they failed.[20]

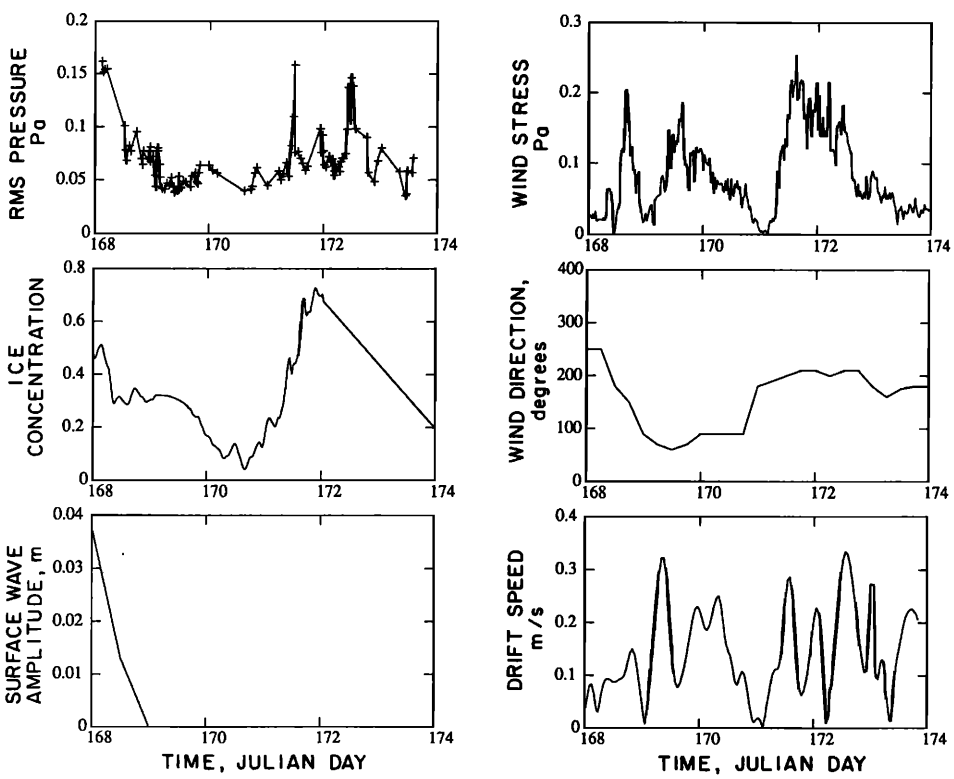

FIG. 4. Noise and various environmental records during the first drift phase: (a) Noise as registered by D6. (b) Ice concentration derived from the STS strain array. Initializations, scaling and interpolations were based upon ice concentration obtained from remote images. (c) Significant wave amplitude, SW, for surface gravity waves incident upon the ice edge with period >8 s. Significant wave amplitude is the amplitude of the 1/3 highest waves.[15] To obtain SW in the MIZ at the acoustic array, at a maximum penetration of 20 km into the ice, multiply the left-hand scale by 0.05. To obtain SW for the full incident spectrum, multiply the left-hand scale by 18. Surface wave amplitude relates to wind stress and wind direction with a time lag the order of 1 day. (d) Wind stress magnitude; see text for conversion from wind speed. (e) Wind vector direction, clockwise from true north. The direction given is the one the wind is pointed toward. (f) Ice drift speed magnitude.

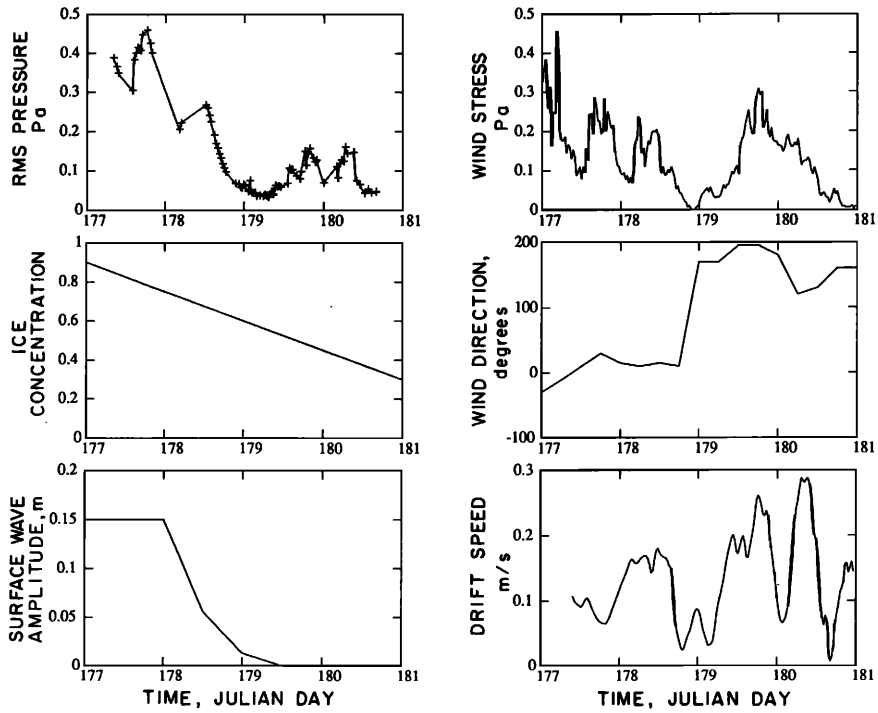

FIG. 5. Noise and various environmental records during the second drift phase: (a) Noise as registered by D6. (b) Ice concentration derived from remote images and field observations. (c) Significant wave amplitude, SW, for surface gravity waves incident upon the ice-edge with period $\geqslant 8$ s. To obtain SW in the MIZ at the acoustic array, at a maximum penetration of 5 km into the ice, multiply the left-hand scale by 0.5. To obtain SW for the full incident spectrum, multiply the left-hand scale by 8. Surface wave amplitude relates to wind stress and wind direction with a time lag the order of 1 day. (d) Wind stress magnitude. (e) Wind vector direction, clockwise from true north. The direction given is the one the wind is pointed toward. (f) Ice drift speed magnitude.

The center frequency of fracture radiation is roughly $f = c_r/L$, where c_r is the Rayleigh wave speed (≈ 1700 m/s) which, for long fracture lengths L ($\geqslant 35$ m) is in the octave band considered. Also, unloading motion radiates at $f = c_g/x_e$, where c_g is the group speed of flexural waves in the ice floe and x_e is the distortion distance; this lies within the range pertinent to our study, $10 < f < 100$ Hz.

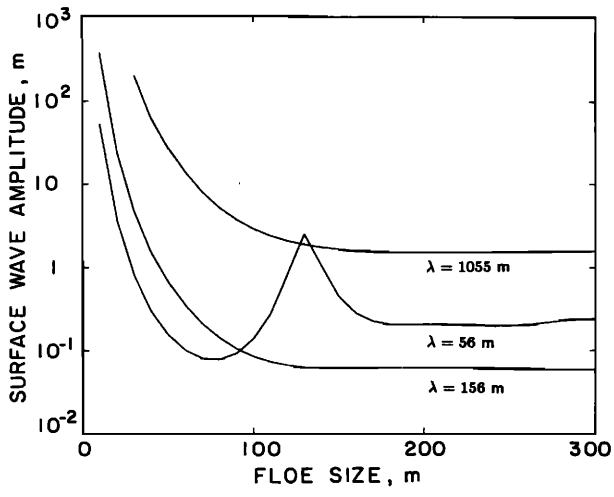

FIG. 6. Minimum significant wave amplitude needed to cause flexural failure in a floe for the given ocean surface wavelength λ and floe length. The values are based upon a model by Goodman *et al.*[17] where the wave responds to an initially rigid floe, upon which the subsequent hydrodynamic pressure field deforms the ice elastically. The ice thickness is taken to be 1.5 m, a critical strain, $\epsilon_{crit} = 4.3 \times 10^{-5}$ and a pre-existing crack length of 10 mm are assumed for failure, based upon observations of real floes in swell.[17] To break MIZ floes, typically of roughly 100-m length, the least surface wave amplitude required is in the swell regime, with wavelengths of roughly 100 to 150 m.

However, it is also possible that low-frequency sound is generated by ice floes in relative motion, as their edges tap against each other. Both horizontal and vertical high-frequency floe collisions in the MIZ are correlated with local swell for amplitudes in excess of $\delta \approx 0.001$ m,[18] the brine layer spacing of sea ice.[21] For smaller wave amplitudes, these edge asperities apparently cause adjacent floes to stick together. We think of δ as the correlation length, in the slide plane, of the asperity roughness. Vibration could then be caused as these asperities slide past each other at frequency $f \approx \mathrm{SW}\omega_{sw}/\delta$, and with $\omega_{sw} \leqslant 1$ rad/s, it can be seen that f is in the low-frequency range of interest.

Finally, it might be thought possible that sound is generated for those larger relative edge motions that cause the asperities to break. The frequency estimate for this is c_a/l, where c_a is the group speed of transverse motion of an asperity of roughness height l and thickness δ. For any reasonable ratio of l/δ, the frequency range of such radiation is much too high to affect our observations.

Considerable evidence to date strongly supports the use of center frequency as a diagnostic for the source mechanism. The reason simply is that an individual fracture, collision, asperity collapse, etc., is known to occupy a bandwidth about equal to the center frequency,[20,22] i.e., about an octave in width. As a relatively narrow-band transient, we are thus justified in using its estimated center frequency to help select the more plausible mechanisms from all those that can be logically proposed for the observation band considered in this paper.

B. Ice field descriptors

Ambient noise was also cross correlated with a variety of ice field descriptors. These include ice concentration, expansion, expansion rate, divergence rate, principal shear

strain rate, rotation rate, and deformation energy. These descriptors were derived from the strain rate tensor of the ice field which was calculated via a linear least-squares method[23] from the relative positions and velocities of eight freely drifting sensors in the STS network. (Position data in the STS network were obtained from raw intersensor time delays, hand edited, linear filtered, and finally averaged over and sampled at 6-min intervals.) This method finds the velocity gradient which minimizes the mean square error between measured velocities of the sensor cluster, and those possible in a linear velocity field. The strain rate tensor is defined as

$$\dot{\epsilon}_{ij} = \frac{1}{2}\left(\frac{\partial u_i}{\partial x_j} + \frac{\partial u_j}{\partial x_i}\right),$$

where $i = a,b$ and $j = a,b$; and where x_a, x_b and u_a, u_b, respectively, are orthogonal positions and velocities in a translating, rotating, horizontal Cartesian frame. The error in the strain rate tensor due to the linearization of the velocity field is no more than 30%. The vorticity of the cluster determined within the Cartesian frame is

$$\dot{\omega} = \frac{1}{2}\left(\frac{\partial u_b}{\partial x_a} - \frac{\partial u_a}{\partial x_b}\right).$$

The divergence rate

$$\dot{\epsilon}_{\text{div}} = \dot{\epsilon}_{aa} + \dot{\epsilon}_{bb},$$

principal shear strain rate

$$\dot{\epsilon}_{12} = \left[\left(\frac{\dot{\epsilon}_{aa} - \dot{\epsilon}_{bb}}{2}\right)^2 + \dot{\epsilon}_{ab}^2\right]^{1/2},$$

and deformation energy

$$(\dot{\epsilon}_{\text{div}})^2 + (\dot{\epsilon}_{12})^2$$

are invariant to rotations of coordinates. The east–west expansion rate (i.e., north–south across ice contraction rate)

$$\dot{\epsilon}_{xx} - \dot{\epsilon}_{yy},$$

where x and y are east and north position coordinates, describes the along-ice-edge expansion rate of the ice field since the orientation of the ice edge is essentially east–west.

The temporal variations of ice concentration and east–west expansion were determined by time integration of the negative divergence rate and east–west expansion rate, respectively. These estimates are presumably stable since these descriptors were obtained from differentiation of the raw position data and are consistent with estimates using subsets of the original STS array. The absolute scale of the ice concentration estimate as well as interpolations made between J171.5 to J174 and J177 to J181 were determined from remote images of the ice edge,[10,24,25] and field observations made by MIT.

The e-folding autocorrelation times of the ice field descriptors are shown in Table IV. Divergence rate, shear strain rate, expansion rate, and vorticity all have e-folding times substantially shorter than that of the noise. These time scales reflect the heterogeneous adjustments of individual floes in the ice field as they respond to environmental forcing. Ice concentration and expansion rate have longer time scales, of the same order as that of wind direction. The longer time scales reflect the homogeneous adjustments of the ice field to variations in wind direction and magnitude.

TABLE IV. Autocorrelation e-folding times for ice field descriptors, in hours. (Data sampled at 6-min intervals.)

	1st drift	2nd drift
$\dot{\epsilon}_{\text{div}}$	1	
$\dot{\epsilon}_{12}$	2	
$\dot{\epsilon}_{xx} - \dot{\epsilon}_{yy}$	1	
C	17	34
$\epsilon_{xx} - \epsilon_{yy}$	89	
ω_{abs}	1	
$\lvert\omega_{\text{abs}}\rvert$	2	
$(\dot{\epsilon}_{\text{div}})^2 + (\dot{\epsilon}_{12})^2$	1	

The noise records were interpolated to a 6-min sampling period to match the higher sampling of the ice field descriptor records. Results of cross correlation between ice field descriptors and noise are summarized in Table V. During the first drift phase, ice concentration correlates best with the noise, but the degree of correlation is not particularly high. An explanation for this will be given in Sec. III since it pertains to noise episodes. Strain rate parameters are all poor correlates of the noise. This is expected, since if the noise is related to floe collisions, strain rates would be high during low ice concentration, when few collisions are possible.

High correlation between ice concentration and noise exists during the second drift phase (although no other ice field descriptors are available due to shut-down of the STS network). The consistency of best correlation with ice concentration in both drift phases suggests two possibilities. First, noise is parametrically dependent upon ice concentration. That is, as ice concentration increases so does the density of potential surface sound sources. Some external forcing, perhaps surface gravity wave interaction with sea ice, may then generate low-frequency sound. Second, the actual convergence of the ice field may cause floes to collide and produce low-frequency sound. For example, in addition to wave-induced floe collision, tapping vibration is also plausible for horizontal collisions resulting from differential wind and current forcing. The differential velocity between floe centers is roughly $s\dot{\epsilon}_{\text{div}}$, where $s = DC^{-1/2}$ is the mean spac-

TABLE V. Cross correlation between ambient noise (rms pressure) in the 25- to 50-Hz band and ice field descriptors. Environmental time series are held fixed. (Data sampled at 6-min intervals.) [Peak correlation coefficient, time lag (h).]

	1st drift $\lvert P\rvert$	2nd drift $\lvert P\rvert$
$\dot{\epsilon}_{\text{div}}$	−0.25, −2.0	
$\dot{\epsilon}_{12}$	0.25, 1.4	
$\dot{\epsilon}_{xx} - \dot{\epsilon}_{yy}$	0.24, 0	
C	0.43, −1.0	0.77, −2.6
$\epsilon_{xx} - \epsilon_{yy}$	−0.15, −1.6	
ω_{abs}	0.29, 0	
$\lvert\omega_{\text{abs}}\rvert$	−0.15, −1.0	
$(\dot{\epsilon}_{\text{div}})^2 + (\dot{\epsilon}_{12})^2$	−0.11, 0	

ing between floe centers and $D = 100$ m is a typical ice floe size for the MIZ. Low-frequency sound would be radiated at $f = D\dot{\epsilon}_{\rm div}/\delta\sqrt{C}$. For the given parameters, and for large values of $C \approx 0.7$ and $\dot{\epsilon}_{\rm div} \leqslant 1.7 \times 10^{-4}\ {\rm s}^{-1}$ as measured during compact conditions, f is less than or roughly equal to 20 Hz and is possibly in the range of interest.

III. HIGH NOISE EPISODES OCCUR DURING WEAK SURFACE WAVE FORCING

During off-ice winds, surface wave activity was weak and episodes of high noise were sometimes observed. These episodes were of roughly 3- to 6-h duration, 1- to 2-h e-folding time, recurred at 12-h periods, but were present only 7% of the time. Portions of the noise record specifically related to these episodes appear in Fig 7.

We cross correlated these portions of the noise record with environmental forcing functions, as summarized in Table VI. Although an argument can be made for wind stress, current stress, and drift acceleration, the best correlate of the noise is consistently drift speed. This is not surprising since drift speed records display substantial 12-h periodicity and have episodes corresponding to those found in the noise, as shown in Fig. 7. The 12-h periodicity in drift speed is likely not caused by tidal current since anomalously strong diurnal, rather than semidiurnal, tides characterize the MIZ near the site of the experiment.[26] Also, current measurements at 50-m depth, where momentum transferred from the surface is minimal, show poor correlation with the noise, suggesting tidal currents are likely unrelated to it. The semidiurnal periodicity in drift speed is more likely related to wind driven inertial oscillations of the ice field. Inertial oscillations can cause oscillating convergence and divergence of the ice field which could result in high noise during periods of increased concentration.

Finer spatial and temporal sampling was available for a particular noise episode. Over a roughly 12-h period at about

TABLE VI. Cross correlation between noise in the 25- to 50-Hz band, specifically related to episodes, and environmental forcing functions. Environmental time series are held fixed. (Data sampled at 1/2 h intervals.) [Peak correlation coefficient, time lag (h).]

	1st drift $\lvert P\rvert$	2nd drift $\lvert P\rvert$
$\lvert\tau_a\rvert$	0.30, 0	0.70, −0.50
$\lvert\tau_w\rvert$	0.60, −0.5	
$\lvert\tau_a + \tau_w\rvert$	0.18, −0.5	
$\lvert\tau_a - \tau_w\rvert$	0.04, −0.5	
$\lvert\mathbf{V}_i\rvert$	0.72, 1.5	0.77, 0.5
$\lvert d\mathbf{V}_i/dt\rvert$	0.6, −1.5	
$\lvert\sigma_p\rvert$	0.51, −2.5	
M_r	0.20, −1.5	
SW	0, 0	−0.18, −1.6
$\lvert\mathbf{V}_g\rvert$	0.25, 2.5	

J171.5, the noise records of seven drifting sensors, averaged at and sampled over a 30-s period, are shown in Fig. 8. A chart of the positions of each sensor during the episode is shown in Fig. 9. Comparing these positions with the noise records, we observe some interesting phenomena. First, sensors furthest to the southeast measure noise of greater amplitude during the episode, suggesting either greater density of sources, greater source strength, or greater proximity to the sound sources. Second, during the episode, sensors within about 1 km of each other measure similar temporal variations, while those measured by sensors at separations greater than 1 km are quite different. Finally, the episode propagated through the array of sensors at roughly 2 to 5 km/h, for a mean of about 3 km/h in a northwest direction.

This propagation speed is an important clue to the episode mechanism. It propagates much too slowly to be an acoustic wave. It is also too slow to be a surface gravity wave

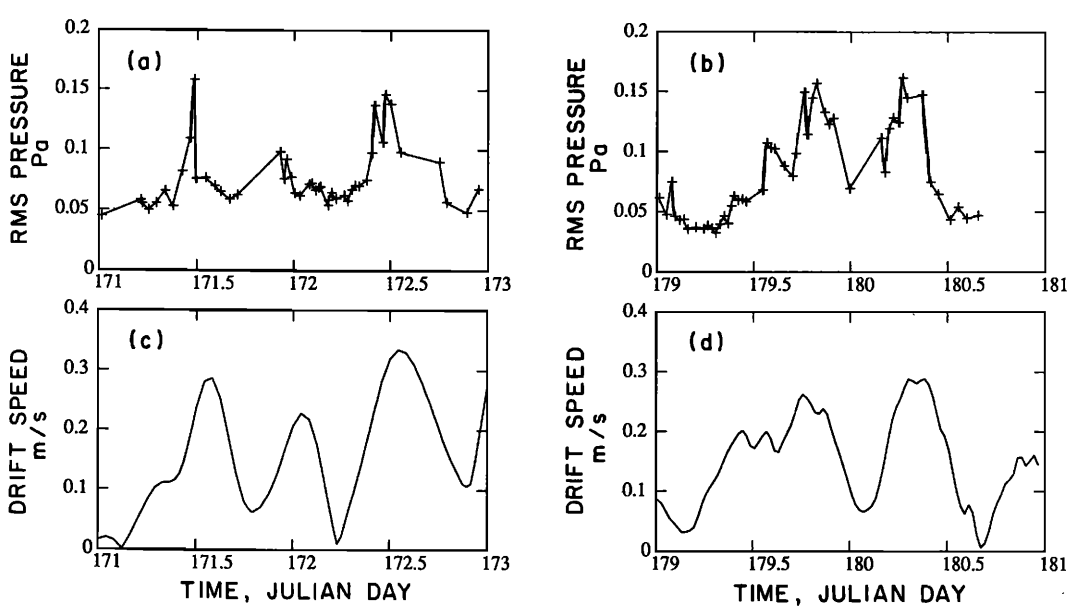

FIG. 7. Records showing high noise episodes during weak surface wave forcing. The episodes are of 3- to 6-h duration and occur during off-ice winds. Two prominent episodes appear during the first drift phase (a) and are separated by a 24-h period. There is evidence of an episode midway between them. Two prominent episodes also appear during the second drift phase (b) and are separated by 12 h. Corresponding ice drift speed records are shown in (c) and (d). Their significance is discussed in the text.

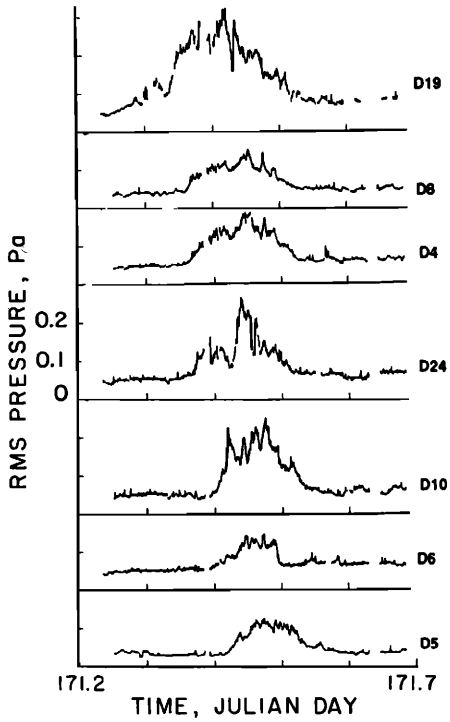

FIG. 8. Records of rms noise in the 25- to 50-Hz band during the episode occurring near J171.5. Corresponding sensors are marked to the right of each record. Records are stacked so that sensors further to the northwest are lower. The episode apparently propagates to the northwest and is of smaller amplitude further to the northwest.

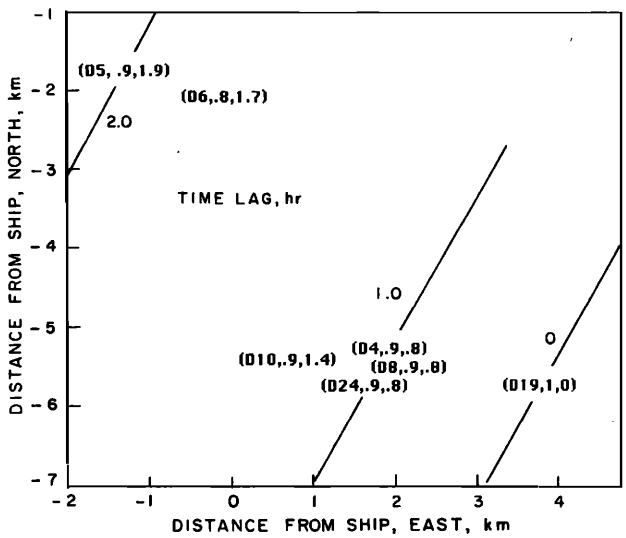

FIG. 9. Chart of the propagation of the J171.5 noise episode through the acoustic array. The relative arrival time of the episode was computed for each sensor by cross correlating each noise record, shown in Fig. 8, with that of the first sensor to detect the episode, D19. The triplets (sensor name, correlation coefficient, time lag in hours) are centered at the position of each sensor during peak correlation. Sensors deviated from the relative positions shown by less than 1 km during the total episodic time of roughly 3 h. Contours have been drawn to show positions of equal time lag of the episode. The episode traveled at roughly 3 km/h to the northwest.

by at least a factor of 5. On the other hand, it is much faster than the drift speed of ice, by at least a factor of 3. However, long internal waves in the Fram Strait MIZ can travel nondispersively with speeds in the range $0.90 < c < 6.8$ km/h, according to Meunch *et al.*,[27] where

$$c = \left(g \frac{\Delta\rho}{\rho} H \right)^{1/2}$$

and where g is the acceleration of gravity, H is the mixed or upper layer thickness defined by the pycnocline, ρ is the mean density of sea water and $\Delta\rho$ is the density jump between upper and lower ocean layers. (Long internal waves have wave numbers k_i such that $k_i H \ll 1$.) The noise episode's propagation speed is within the range of long internal waves. Also, the speeds are consistent with density jump and mixed layer thickness measured during MIZEX 84.[28] Therefore, we conclude that this particular noise episode is affected by the passage of long internal waves.

Meunch *et al.* speculate that long internal waves may be generated at the ice edge during off-ice wind forcing, and this coincides with the conditions during which we observed noise episodes. They further speculate that these internal waves may concentrate the ice field into bands of high concentration due to alternating convergence and divergence zones created at the sea surface along the wave's path.[29]

We speculate that the propagating noise episode is due to the advection of bands of highly concentrated ice by a long internal wave. We further speculate that the other noise episodes observed were also related to the formation of bands of highly concentrated ice by internal waves. Additional support for this appears in Fig. 10. Bands of high ice concentration appear in the vicinity of the acoustic array at the same time of day as the noise episodes which occurred two and three days earlier, and, as Fig. 4 shows, during which the surface waves remain equally weak. The spacing, width and orientation of the bands suggest the propagation of a long internal wave in roughly the same direction as the noise episode.

The weaker correlation between ice concentration and noise found during the first drift phase, in comparison with the second, is likely due to the inability of the strain array to resolve the smaller scale ice bands which we speculate to have affected the noise episodes.

IV. SUMMARY AND DISCUSSION

We have studied low-frequency ambient noise records measured under drifting ice floes of the Fram Strait MIZ under early summer conditions. We find that long term variations of the noise are strongly related to the amplitude of open ocean surface gravity waves incident on the ice edge. In this, we confirm the conclusion of earlier researchers,[2] who attributed MIZ noise to surface gravity waves interacting with the floes. We also find that these long term variations of the noise are related to ice concentration which, in turn, is determined primarily by wind-induced free-drift of the ice. While ice drift exhibits semidiurnal inertial oscillations, noise associated with surface wave forcing has at most weak semidiurnal components. The noise under surface wave forcing is, instead, created and integrated over large spatial

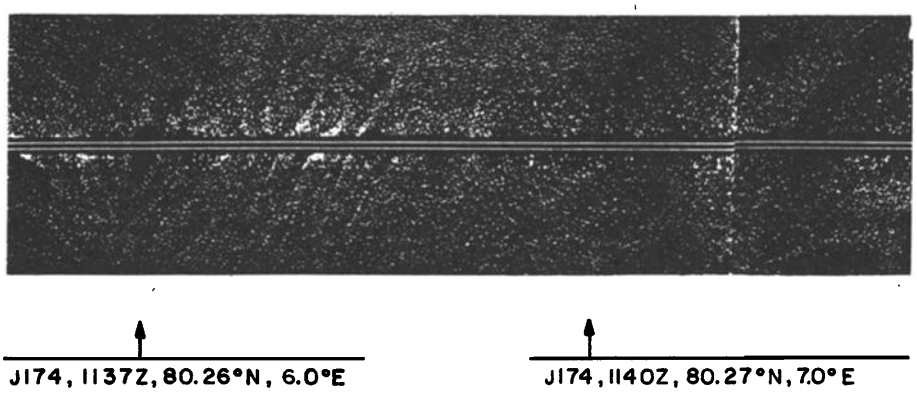

FIG. 10. A side-looking airborne radar image at 19 GHz taken during a NOAA P3 flight over the ice-edge at about J174.5.[25] The swath width is roughly 11 km and the distance between the arrows on the horizontal is 19 km. The Kvitbjorn is located at 80.26° N 7.4° E, which is just off the image to the east. The white specks are ice floes of roughly 100 to 200 m in size, and the ice concentration is between 0.2 to 0.4 except where bands of roughly 1- to 2-km spacing, 1-km width and 2- to 3-km length appear centered at 80.3° N between 6.2° and 6.5° E, where much higher concentrations are found. (The vertical line at about 7.3° E is due to splicing of the image. It does not represent an actual ice band.)

(≥5 km) and temporal (≥3 h) scales, where the numerical values come from measured correlations.

Shorter spatial and temporal scales can also be observed in the data, and while the noise at such scales occurs infrequently and is therefore of less practical importance, its study leads to confirmation of important physical ideas. Brief episodes of high noise were detected during off-ice winds and correspondingly weak surface wave amplitudes. These episodes are of roughly 1 h *e*-folding time, of semidiurnal periodicity, and are strongly related to ice drift speed, which also is semidiurnal. Because such episodes propagate at a speed consistent with internal waves, we speculate that they are additionally affected by the formation and advection of bands of high ice concentration by internal waves formed at the ice edge during off-ice winds. Thus ice concentration has a twofold effect in episodic behavior, first via semidiurnal inertial oscillations of the ice floes in free drift, and second via ice banding driven by long internal waves. Such ice concentration effects combine to give relatively shorter spatial and temporal scales to the noise than that caused by on-ice surface gravity waves. When the latter are present, the wind is expected to be on ice, and the presumed generation mechanism for long internal waves would be absent, as would the episodes in the form observed.

We conclude for both long and short scales that ice concentration is an important parameter of MIZ noise. It determines not only the spatial and temporal scales, but also indirectly the magnitude of the noise. In this sense, earlier observations of MIZ hotspots attributed to ice-edge eddies[3,4] are likely of the same class as the observations here, the eddy merely imposing spatial and temporal scales characteristic of its dynamics, in contrast to the ice-edge dynamics observed in the present study.

It should be no surprise that a stress parameter, such as imposed by incident surface gravity waves, and a strain parameter, such as ice concentration, jointly relate to MIZ ambient noise. In the MIZ, stress and strain are uncoupled; no constitutive law for the field can exist under free-drift conditions. Further, we have focused on the one best correlate for each stress or strain parameter. It is likely that multivariate analyses in each would provide firmer knowledge of MIZ ambient noise, but some useful physical knowledge can nonetheless be extracted from the narrower focus in our study.

From data in our study, we can assess the plausibility, at least to first order, of the actual mechanisms by which low-frequency sound is generated in the MIZ. Because surface gravity wave amplitude is the best noise correlate for large spatial/temporal scales, physical mechanisms should be invoked involving it. First, incoming waves can cause flexural fracture in ice floes, and second, they can cause relative vertical and horizontal motion between adjacent floes. The first radiates noise directly from each fracture, and subsequently from unloading motion as each fractured floe returns to its undeformed state.[20,22] The second radiates noise as asperities on edges of adjacent floes in contact break or vibrate in response to relative floe motion. For the present study, surface wave amplitudes within several kilometers of the ice-edge were sufficient to cause floe fracture and asperity breaking or vibration. The frequency range within which flexural fracture and unloading motion creates noise is estimated to easily cover the low-frequency range of interest. Asperity vibration can cover portions of this range at the lowest end, but asperity breaking is too high in frequency. So we nominate flexural fracture and asperity vibration as the plausible mechanisms. Flexural fracture, however, is much more likely, not only because of its broader frequency coverage, but also because much larger energy is invested in a floe to fracture rather than to vibrate it, with noise radiation therefore larger.

Small scale variations of the noise, as in episodes, are unrelated to surface waves. It is possible that floe collision in ice convergence is responsible, but we estimate that this mechanism covers the range only for $f < 20$ Hz (see comment at the end of Sec. II B). The restricted frequency range, plus the low overall correlation of $\dot{\epsilon}_{\text{div}}$ with the noise (see Table V), prevents us from labeling this mechanism as plausible. While the source mechanism thus remains unsettled for small scale variations, we do not have a better candidate than floe collision in ice convergence.

ACKNOWLEDGMENTS

We are sincerely grateful to the many people at MIT and WHOI who were responsible for the acquisition of acoustic and STS data during MIZEX 84. We extend special thanks to Dr. Gregory L. Duckworth for his assistance during the reduction of the STS data, and for offering many valuable comments and suggestions during the course of this work.

This work was sponsored in part by the ONR Arctic Program Office.

APPENDIX

To obtain quantitative measurement of temporal scales and the linear relationship between time series, a cross-correlation algorithm was devised that requires no interpolation of data gaps and so introduces no hypothetical information. Time series had only to be resampled to a consistent sample period upon which gaps were reintroduced. For each lag, discrete correlation coefficients could be computed by summing only overlapping samples and so ignoring gap–gap and gap–sample overlaps in the convolution. Time series in each lag window were locally "zero-meaned" and normalized by the square root of the variance product of each time series using only nonzero overlap samples in the local lag window. Even a time series with no gaps would require a moving normalization window to account for the nonstationarity inherent in data streams of finite length. The scheme is symbolically described below.

The ideal time series with no data gaps are $x[n]$ and $y[n]$, of lengths N_x and N_y, respectively. Time series $\delta_x[n]$ and $\delta_y[n]$ are zero for data gaps at n such that $\delta_x[n]x[n]$ and $\delta_y[n]y[n]$ are the actual time series with data gaps.

The cross-correlation function is then

$$R_{xy}(m) = \sum_{n=0}^{N_x} \frac{(x[n]-\bar{x}[m])(y[a]-\bar{y}[m])\delta_x[n]\delta_y[a]}{\sigma_x[m]\sigma_y[m]N[m]},$$

for

$$0 \leqslant m \leqslant N_x + N_y - 1, \quad a = n - [m - (N_y - 1)],$$

where

$$\bar{x}[m] = N^{-1}[m] \sum_{n=0}^{N_x} x[n]\delta_x[n]\delta_y[a],$$

$$\bar{y}[m] = N^{-1}[m] \sum_{n=0}^{N_x} y[a]\delta_x[n]\delta_y[a],$$

$$\sigma_x^2[m] = N^{-1}[m] \sum_{n=0}^{N_x} x^2[n]\delta_x[n]\delta_y[a] - (\bar{x}[m])^2,$$

$$\sigma_y^2[m] = N^{-1}[m] \sum_{n=0}^{N_x} y^2[a]\delta_x[n]\delta_y[a] - (\bar{y}[m])^2,$$

$$N[m] = \sum_{n=0}^{N_x} \delta_x[n]\delta_y[a].$$

The same procedure was used for all correlations in this paper.

[1] N. C. Makris, and I. Dyer, "Environmental correlates of pack ice noise," J. Acoust. Soc. Am. **79**, 1434–1440 (1986).

[2] O. I. Diachok and R. S. Winokur, "Spatial variability of underwater ambient noise at the Arctic ice-water boundary," J. Acoust. Soc. Am. **55**, 750–753 (1974).

[3] T. C. Yang, C. W. Votaw, G. R. Giellis, and O. I. Diachok, "Acoustic properties of ice edge noise in the Greenland Sea," J. Acoust. Soc. Am. **82**, 1034–1038 (1987).

[4] O. M. Johannesen, S. G. Payne, K. V. Starke, and G. A. Gotthard, I. Dyer, "Ice eddy ambient noise," in *Sea Surface Sound*, edited by B. Kerman, NATO ASI Series (Kluwer Academic, Boston, 1988), pp. 599–605.

[5] J. K. Lewis and W. W. Denner, "Higher frequency ambient noise in the Arctic Ocean," J. Acoust. Soc. Am. **84**, 1444–1455 (1988).

[6] K. Von der Heydt, G. L. Duckworth, and A. B. Baggeroer, "Acoustic array tracking system," in Proceedings of the IEEE on Oceans, San Diego, CA (1985).

[7] G. L. Duckworth, "A robust algorithm for tracking of drifting acoustic arrays in the Arctic," in *Signals, Systems and Computers* (Twenty First ASILOMAR Conference Proceedings, Pacific Grove, CA, 1987).

[8] O. M. Johannessen, J. A. Johannessen, E. Svendsen, R. A. Schuchman, W. J. Campbell, and E. Josberger, "Ice edge eddies in the Fram Strait Marginal Ice Zone," Science **236**, 427–429 (1987).

[9] T. O. Manley, J. Z. Villaneuva, J. C. Gascard, P. F. Jeannin, K. L. Hunkins, and J. van Leer, "Mesoscale oceanographic processes beneath the ice of Fram Strait," Science **236**, 432–434 (1987).

[10] W. J. Campbell, P. Gloersen, E. G. Josberger, O. M. Johannessen, P. S. Guest, N. Mognard, R. Shuchman, B. A. Burns, N. Lannelongue, and K. L. Davidson, "Variations of mesoscale and large-scale sea ice morphology in the 1984 Marginal Ice Zone Experiment as observed by microwave remote sensing," J. Geophys. Res. **92**, 6805–6824 (1987).

[11] N. C. Makris, "Environmental correlates of Arctic ice edge noise," Thesis, MIT, Cambridge, MA (1990).

[12] P. Guest and K. L. Davidson, "The effect of observed ice conditions on the drag coefficient in the summer East Greenland Sea Marginal Ice Zone," J. Geophys. Res. **92**, 6943–6954 (1987).

[13] S. Sandven, E. Svendsen, and O. M. Johannessen, "MIZEX 84 current, temperature and salinity measurements from drifting ice floes," University of Bergen, Norway (1985).

[14] G. A. Maykut and D. K. Perovich, "The role of short wave radiation in the summer decay of a sea ice cover," J. Geophys. Res. **92**, 7032–7044 (1987).

[15] W. J. Pierson, G. Neumann, and R. W. James, "Practical methods for observing and forecasting ocean waves by means of wave spectra and statistics," US Naval Oceanographic Office (1967).

[16] P. Wadhams, V. A. Squire, D. J. Goodman, A. M. Cowan, and S. C. Moore, "The attenuation rates of ocean waves in the Marginal Ice Zone," J. Geophys. Res. **93**, 6799–6818 (1988).

[17] D. J. Goodman, P. Wadhams, and V. A. Squire, "The flexural response of a tabular ice island to ocean swell," Annal. Glaciology **1**, 23–27 (1980).

[18] S. Martin and P. Becker, "High frequency ice floe collisions in the Greenland Sea during the 1984 Marginal Ice Zone Experiment," J. Geophys. Res. **92**, 7071–7084 (1987).

[19] O. Diatchok, "Arctic hydroacoustics," Cold Regions Science Technol. **2**, 185–201 (1980).

[20] I. Dyer, "Speculations on the origin of low frequency Arctic Ocean noise," in *Sea Surface Sound*, edited by B. Kerman, NATO ASI Series, (Kluwer Academic, Boston, 1988), pp. 513–532.

[21] W. F. Weeks and M. Mellor, "Mechanical properties of ice in the Arctic Seas," in *Arctic Technology and Policy*, edited by I. Dyer and C. Chryssostomidis (Hemisphere, New York, 1983) pp. 235–260.

[22] C. Chen, "An analysis of Marginal Ice Zone noise events," Thesis, MIT, Cambridge, MA (1990).

[23] W. D. Hibler, III, W. F. Weeks, A. Kovacks, and S. F. Ackley, "Differential sea ice drift, I: spatial and temporal variations in sea ice deformation," J. Glaciology **13**(69) (1974).

[24] J. H. Morison, M. G. Mcphee, and G. A. Makykut, "Boundary layer, upper ocean, and ice observations in the Greenland Sea Marginal Ice Zone," J. Geophys. Res. **92**, 6987–7011 (1987).

[25] D. Ross, image for NOAA P3C flight June 22 1984, Cooperative Institute for Marine and Atmospheric Studies. Informal memorandum transmitted to MIT in 1985.

[26] K. L. Hunkins, "Anomalous diurnal tidal currents on the Yermak Plateau," J. Mar. Res. **44**, 51–69 (1986).

[27] R. D. Muench, P. H. Leblond, and L. E. Hachmeister, "On some possible interactions between internal waves and sea ice in the Marginal Ice Zone," J. Geophys. Res. **88**, 2819–2826 (1983).

[28] S. Sandven, E. Svendsen, O. M. Johannessen, and J. A. Johannessen, "A CTD report from the Marginal Ice Zone Experiment in the Fram Strait between Svalbard and Greenland in June–July 1984," University of Bergen, Norway, Vol. 5 (1985).

[29] A. E. Gill, *Atmosphere-Ocean Dynamics* (Academic, San Diego, 1982).